## Variation in fault core properties and its impact on fault seal behaviour

### Introduction

Faults can act as potential pathways for lateral or vertical migration of fluids and serve as efficient flow barriers (Caine et al., 1996). As faults are ubiquitous structures in sedimentary basins, evaluating fault seal behaviour is essential for ensuring the safety of subsurface carbon storage operations (Miocic et al., 2019). The rapid scale-up of Carbon Capture and Storage (CCS) infrastructure is one of the key strategies to accelerate decarbonization efforts for achieving global reduction in anthropogenic carbon dioxide emissions to the atmosphere. In this context, a comprehensive understanding of geological processes at fault zones is crucial to refine thumb rules utilized to ensure the seal integrity of $CO_2$ storage sites. Variations in the fault rock composition and the associated changes in wettability properties play an important role in influencing the trapping of $CO_2$ (Miocic et al., 2019). While borehole data and drilled cores offer limited access to subsurface fault zones, well-preserved outcrops of exhumed fault zones that cut through reservoir and cap rocks offer a unique opportunity for detailed, integrated investigations of fault rock materials, providing critical insights for subsurface understanding. Additionally, although extensive studies have examined the variation in rock properties from the undeformed wall rock to the fault core in siliciclastic and carbonate rocks (Torabi et al., 2020a 2020b, 2026), there remains a limited understanding of the changes in rock properties within the fault core fabric itself and the inter-relationships between elastic, petrophysical and mineralogical characteristics. The fault core represents the localized zone of deformation formed during faulting (Caine et al., 1996; Torabi et al., 2020b). A thorough understanding of the complex three-dimensional geometry of fault core fabric together with the associated inter-relationships of rock properties within the fault core are critical for constructing realistic fault models in reservoir simulation for $CO_2$ storage. This study presents newly acquired datasets from detailed outcrop investigations in Granada Basin, Spain - providing constraints that can aid in building realistic reservoir simulation models for fault seal analysis relevant to $CO_2$ storage.

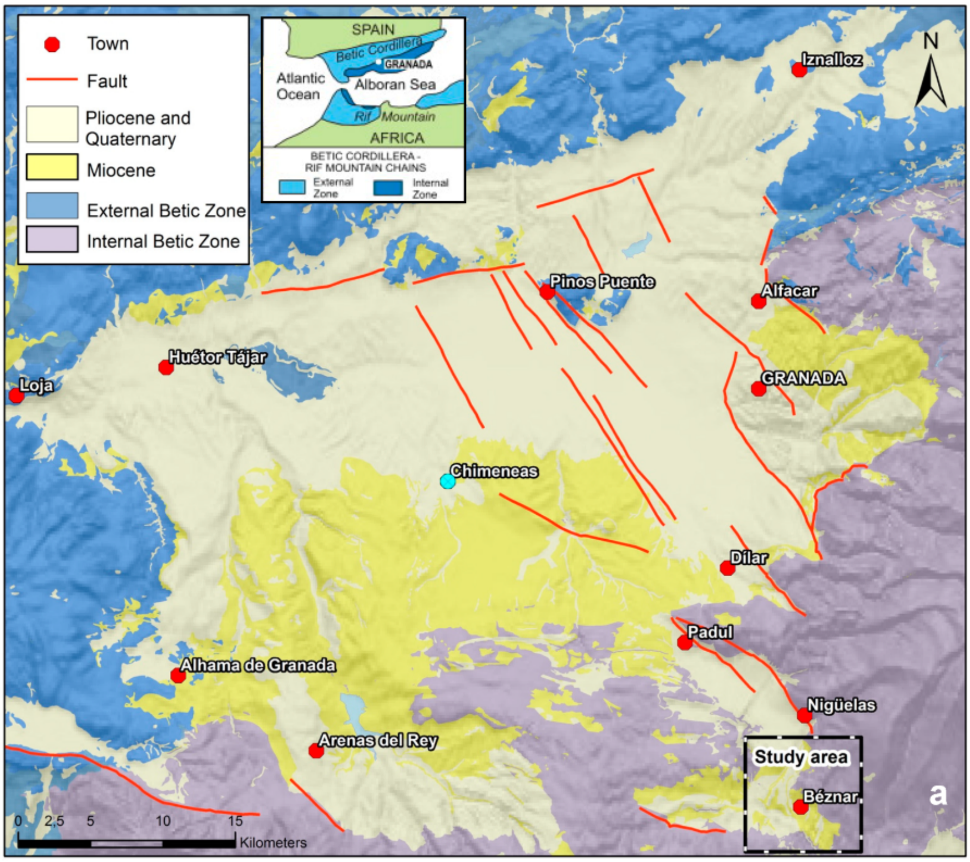

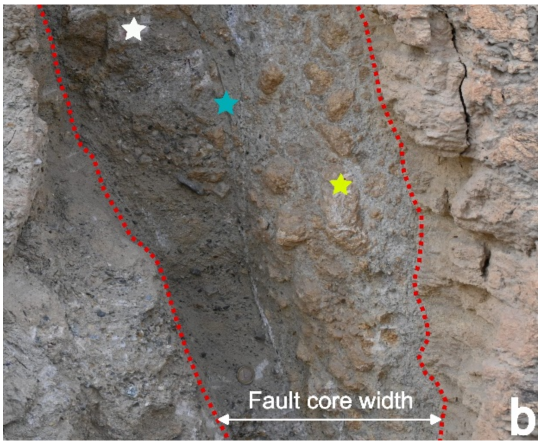


*Figure 1 (a) Geological map of the Granada Basin, southern Spain (Torabi et al., 2020b). (b) Outcrop picture of fault core showing locations of fault core elements (from left to right – fault breccia, fault gouge and host rock lens), where in-situ measurements of Young's Modulus, permeability and elemental oxide counts from XRF were taken (coin for scale). Refer to T1 locations in Table 1 for the datasets.*

The study area is in the southeastern part of Neogene-Quaternary Granada Basin, Southern Spain, where faults cut across ~80m thick clay-bearing conglomerates and ~30-40m-thick carbonate grainstones containing cm-thick microconglomerate and sand interbeds (Agosta et al., 2012) (Fig. 1a). There are three major sets of faults striking ~N-S, E-W and NW-SE with throws up to 100m, 80m and 100m, respectively (Torabi et al., 2020b).

**Methodology**

We conducted scanline analysis oriented orthogonal to the fault strike at 4 separate fault zones (T1, T2, T3 and T4) along the road section near Tablate locality. The structural elements of the fault core were categorized as fault gouge, fault breccia, clay smear and host rock lens (within the fault core) following the classification of Torabi et al., 2020b and Muñoz et al., 2026. In-situ measurements were collected from the fault core fabric as well as the immediately adjacent host rocks. Young's Modulus was estimated from rebound values of Schmidt hammer using the approach described by Katz et al. (2000). A portable digital air permeameter, TinyPermIII developed by New England Research was used to measure permeability. Geochemical analyses were conducted by positioning a Bruker TITAN handheld X-ray fluorescence (XRF) analyzer on a fresh outcrop surface for 60 seconds. The device delivers raw counts of major element oxides, which show a linear correlation with weight percent (Young et al., 2016; Muñoz et al., 2026). These devices were placed along the strike of the fault and bedding plane due to better accessibility of such sections in the studied outcrops. Building on the background of the dominant minerals identified in these rocks through XRD analyses by Torabi et al (2020b), we utilized the ratios of raw counts of major elemental oxides – Si/(Mg + Ca) to assess the relative abundance of siliceous and carbonate mineral components and (Al + K)/(Ca +Mg) to estimate the probable dominance of phyllosilicates versus carbonates. To preliminarily separate the contributions of MgO to phyllosilicates (particularly in the case of chlorite group minerals) and dolomites, we measured the ratio of Mg/Ca, as both these oxides are also key components of dolomite. The inferences from the ratios of major elemental oxides are compared to the measured permeability and Young's Modulus values in both faults as well as host rocks.

**Results**

The dominant orientation of the fault core at all the 4 studied sites, where in-situ measurements were taken was ~60/235. The thickness of the fault core varied from ~17cm to ~48cm. The structural elements within the fault core exhibited a variation of permeability between lower estimates of 0.14 mD in the phyllosilicate-rich fault gouge to 678.16 mD in the host rock lens (very poorly sorted fabric entrained within the fault core with conglomerate clasts) (Table 1, Figure 2). Lower permeability values were also found in lenses of host rocks within the fault core, where there was evidence of strong calcite cementation and dominance of calcite over silicic components. This was inferred from lower values of the oxides of Si/(Mg + Ca), (Al + K)/(Ca +Mg) and Mg/Ca (Table 1). The host rocks showed a variation of permeability values between 0.103 mD (strongly cemented by calcite) and 647.8 mD. Similar to the host rock lens within the fault core, the host rocks showing higher values of permeability consisted of conglomerate clasts in a very poorly sorted fabric. Additionally, host rocks with strong calcite cementation with low silicic inputs exhibited low permeability and high Young's Modulus (Table 1, Figure 2). This variation in petrophysical and geomechanical properties will influence the sealing behaviour of the fault during $CO_2$ injection. Our detailed analysis suggests that mineralogy as well as the grain-size distribution play an important role in governing the rock properties within the fault core and the adjacent host rocks. Such insights can be useful while predicting fault rock composition and their properties in the subsurface.

| Location | Description | Si/(Ca+Mg) | (Al+K)/(Ca+Mg) | Mg/Ca | *K* (mD) | *E* (GPa) |
|---|---|---|---|---|---|---|
| T1a | Fault gouge - fine-grained dark unit | 8.73 | 1.48 | 2.75 | 0.36 | 3.31 |
| T1b | Breccia | 10.58 | 2.64 | 0.81 | 441.20 | 1.39 |
| T1c | Host rock lens (conglomeratic) | 4.19 | 1.03 | 0.31 | 678.16 | 0.62 |
| T1d | Host rock-sand-silt | 6.46 | 1.63 | 0.35 | 503.13 | 0.65 |
| T1e | Host rock - conglomeratic (finer than T1f) | 6.11 | 1.94 | 0.59 | 80.40 | 0.90 |
| T1f | Host rock - conglomeratic (coarser than T1e) | 2.91 | 0.75 | 0.19 | 647.80 | 2.35 |
| T1g | Host rock -well cemented | 0.69 | 0.21 | 0.14 | 0.10 | 14.91 |
| | | | | | | |
| T2a | Fault gouge | 9.12 | 2.00 | 1.15 | 9.93 | 1.60 |
| T2b | Breccia (not-cemented, partly fine-grained) | 2.46 | 0.43 | 0.12 | 20.43 | 2.01 |
| T2c | Breccia (cemented) | 1.47 | 0.38 | 0.29 | 65.30 | 2.87 |
| T2d | Host rock lens | 0.20 | 0.09 | 0.06 | 0.39 | 3.16 |
| T2e | Breccia (poorly cemented) | 4.11 | 1.03 | 0.18 | 150.80 | 0.51 |
| T2f | Host rock - conglomerate | 2.39 | 0.49 | 0.27 | 282.46 | 0.18 |
| T2g | Host-rock-layered limestone | 0.54 | 0.18 | 0.12 | 2.36 | 8.10 |
| | | | | | | |
| T3a | Fault gouge - cemented | 4.01 | 0.75 | 0.87 | 19.06 | 1.51 |
| T3b | Breccia | 2.85 | 0.55 | 0.64 | 26.56 | 3.09 |
| T3c | Host rock lens | 0.33 | 0.13 | 0.05 | 1.33 | 2.48 |
| T3d | Host rock | 1.29 | 0.27 | 0.10 | 4.30 | 4.23 |
| T3e | Host rock-Sandy-Coarse-grained | 1.47 | 0.24 | 0.52 | 11.85 | 2.29 |
| T3f | Host-rock - similar to host rock lens - T3c | 0.52 | 0.18 | 0.09 | 2.00 | 5.19 |
| | | | | | | |
| T4a | Fault gouge | 6.15 | 1.07 | 0.56 | 0.14 | 1.65 |
| T4b | Breccia/more with clay smear | 9.14 | 1.76 | 1.34 | 106.93 | 0.46 |
| T4c | Breccia | 12.04 | 2.22 | 0.64 | 53.20 | 0.39 |
| T4d | Clay smear close to FW | 5.49 | 0.92 | 1.48 | 0.96 | 0.62 |
| T4e | Host rock lens within fault core | 8.32 | 1.68 | 0.57 | 73.00 | 0.37 |
| T4f | Host rock | 3.32 | 0.82 | 0.70 | 118.80 | 0.29 |
| T4g | Host rock | 4.20 | 1.27 | 0.45 | 135.63 | |
| T4h | Host rock | 10.84 | 2.76 | 1.15 | 131.86 | |

Table 1. Table showing the location, description of the site of investigation, ratios of major elemental oxides, permeability (*K*) and Young's Modulus (*E*).

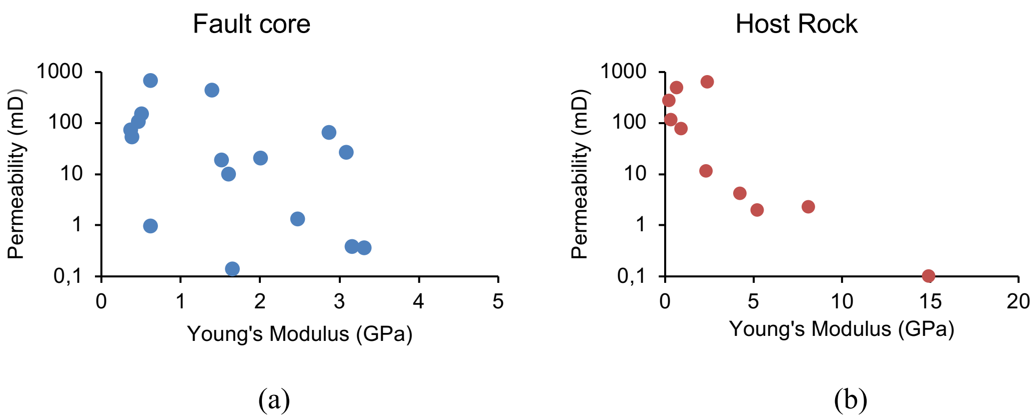


*Figure 2 Plots showing the variation of Permeability with Young's Modulus in fault core & host rocks*

## Conclusion

This study investigates underexplored aspects of fault core properties and their interrelationships, highlighting the value of integrated studies using high-quality outcrops to establish constraints for inferring subsurface fault rock variations and their causes. It emphasizes the role of non-destructive techniques in understanding geological processes within fault zones. Results show that fault core permeability can vary by over four orders of magnitude, influenced by mineralogy, grain size, and host rock interactions. Significant permeability reduction occurs due to clay or calcite concentration in fault gouge or entrained host rocks. Conversely, poorly sorted host rock lenses within the fault core exhibit high permeability. These factors contribute to a broad permeability range, impacting fault seal behavior. The integrated approach used in this study can help in optimizing the upscaling process by balancing the knowledge of the complex fault rock properties with an understanding of broader geological processes relevant at larger scales, ultimately ensuring a more accurate understanding of the subsurface.


## Acknowledgements

These results have been produced with financing from FME gigaCCS administered by The Research Council of Norway (350370) and CO2SafeQuest Project with project number 354868 funded by The Research Council of Norway through CETP CCUS program.


## References


Agosta, F., Ruano, P., Rustichelli, A., Tondi, E., Galindo-Zaldívar, J., & de Galdeano, C. S. [2012]. Inner structure and deformation mechanisms of normal faults in conglomerates and carbonate grainstones (Granada Basin, Betic Cordillera, Spain): Inferences on fault permeability. *Journal of Structural Geology*, *45*, 4-20.

Caine, J. S., Evans, J. P., & Forster, C. B. [1996]. Fault zone architecture and permeability structure. *Geology*, *24*(11), 1025-1028.

IPCC: IPCC Special report on Carbon Dioxide Capture and Storage, Cambridge University Press, New York, USA Cambridge, UK, 2005.

Katz, O., Reches, Z. E., & Roegiers, J. C. [2000]. Evaluation of mechanical rock properties using a Schmidt Hammer. *International Journal of rock mechanics and mining sciences*, *37*(4), 723-728.

Miocic, J. M., Johnson, G., & Bond, C. E. [2019]. Uncertainty in fault seal parameters: implications for CO 2 column height retention and storage capacity in geological $CO_2$ storage projects. *Solid earth*, *10*(3), 951-967.

Muñoz, J. M., Torabi, A., Basa, A., Hansen, T., & Skurtveit, E. [2026]. Fault-core in overburden section: geomechanical and geo-chemical characterisation of the Baza fault core, southern Spain. In *2nd Caprock Integrity & Gas Storage Symposium 2026* (p. 41).

Torabi, A., Ellingsen, T. S. S., Johannessen, M. U., Alaei, B., Rotevatn, A., & Chiarella, D. [2020]. Fault zone architecture and its scaling laws: where does the damage zone start and stop?.

Torabi, A., Jiménez-Millán, J., Jiménez-Espinosa, R., García-Tortosa, F. J., Abad, I., & Ellingsen, T. S. [2020]. Effect of mineral processes and deformation on the petrophysical properties of soft rocks during active faulting. *Minerals*, *10*(5), 444.

Torabi, A., Alaei, B., Basa, A., Jiménez-Millán, J., Jiménez Espinosa, R., García-Tortosa, F. J., & Abad, I. [2026]. *Integrated characterization of an active fault, insights from fault geometry, roughness and properties*. *Physics and Chemistry of the Earth, Parts A/B/C, 143*, Article 104346.